White Rose Research Online

eprints@whiterose.ac.uk
https://eprints.whiterose.ac.uk
Universities of Leeds, Sheffield and York

Deposited via The University of York.

White Rose Research Online URL for this paper:
https://eprints.whiterose.ac.uk/id/eprint/223159/

Version: Accepted Version

Article:
Vikas, Kathuria, Lakshay, Brodie, Claire N et al. (2025) Selective PNP Pincer-Ir Promoted Acceptorless Transformation of Glycerol to Lactic Acid and Hydrogen. Inorganic Chemistry. pp. 3760-3770. ISSN: 0020-1669

https://doi.org/10.1021/acs.inorgchem.4c04580

Reuse
This article is distributed under the terms of the Creative Commons Attribution (CC BY) licence. This licence allows you to distribute, remix, tweak, and build upon the work, even commercially, as long as you credit the authors for the original work. More information and the full terms of the licence here:
https://creativecommons.org/licenses/

Takedown
If you consider content in White Rose Research Online to be in breach of UK law, please notify us by emailing eprints@whiterose.ac.uk including the URL of the record and the reason for the withdrawal request.

UNIVERSITY OF LEEDS
University of Sheffield
UNIVERSITY of York

This document is confidential and is proprietary to the American Chemical Society and its authors. Do not copy or disclose without written permission. If you have received this item in error, notify the sender and delete all copies.

Selective PNP Pincer-Ir Promoted Acceptorless Transformation of Glycerol to Lactic Acid and Hydrogen

Journal:	*Inorganic Chemistry*
Manuscript ID	ic-2024-04580h.R2
Manuscript Type:	Article
Date Submitted by the Author:	05-Feb-2025
Complete List of Authors:	Vikas, *; Indian Institute of Technology Guwahati, Department of Chemistry Kathuria, Lakshay; Indian Institute of Technology Guwahati, Department of Chemistry Brodie, Claire; University of York, Chemistry Cross, Mathew; University of York, Chemistry Pasha, Farhan; SABIC Corporate Research And Devlopment Center, Computational Chemistry Weller, Andrew; University of York, Chemistry Kumar, Akshai; Indian Institute of Technology Guwahati, Department of Chemistry

SCHOLARONE™
Manuscripts

Selective PNP Pincer-Ir Promoted Acceptorless Transformation of Glycerol to Lactic Acid and Hydrogen

Vikas,[a] Lakshay Kathuria,[a] Claire N. Brodie,[b] Mathew J. Cross,[b] Farhan Ahmad Pasha,[c] Andrew S. Weller,*[b] and Akshai Kumar*[a,d,e]

[a] Department of Chemistry, Indian Institute of Technology Guwahati, Guwahati – 781039, Assam, India

[b] Department of Chemistry, University of York, York YO10 5DD, UK

[c] SABIC, Corporate Research and Development, King Abdullah University of Science and Technology, Thuwal-23955, KSA

[d] Center for Nanotechnology, Indian Institute of Technology Guwahati, Guwahati – 781039, Assam, India

[e] Bhupat Mehta School of Health Science and Technology, Indian Institute of Technology Guwahati, Guwahati – 781039.

KEYWORDS. Pincer-Ir Catalysts, Mechanistic Studies, Glycerol, Lactic Acid, Dehydrogenation.

ABSTRACT: The catalytic transformation of glycerol (GLY) using [(^{i}Pr2PN^{H}P)Ir(COD)]Cl [^{i}Pr2PN^{H}P = κ^3-(^{i}Pr$_2$PCH$_2$CH$_2$)$_2$NH] affords hydrogen and lactic acid (LA), trapped as its sodium salt (Na[LA]) with high yield (96%) and selectivity (99%) in the presence of an equivalent of *in-situ* generated NaOEt at 140 °C within 4 h. A diminution in activity was observed when PN^{Me}P ligand was used instead of PN^{H}P, or when Cl^{-} was replaced by [BAr$^{F}_4$]$^{-}$. An Ir to Rh substitution also resulted in poor activity. Kinetic studies show a first-order dependence of the initial-rate on the concentrations of [(^{i}Pr2PN^{H}P)Ir(COD)]Cl, NaOEt and glycerol. An outer-sphere mechanism does not explain the activity of [(^{i}Pr2PN^{Me}P)Ir(COD)]Cl, and DFT studies support an inner-sphere mechanism, with oxidative addition of glycerol to a 14-electron intermediate [(^{i}Pr2PN^{H}P)Ir]Cl as the rate-determining step (RDS). A KIE of 2.7 obtained with glycerol-D$_8$, shows a major contribution from O–H activation in the RDS. The kinetics of the reaction become favorable ($\Delta G_{140}^{\ddagger}$ = 27.01 kcal/mol) when one of the terminal O–H's of glycerol is hydrogen-bonded to the N–H of the pincer backbone, in contrast to cases where no hydrogen bonds are invoked ($\Delta G_{140}^{\ddagger}$ = 31.96 kcal/mol) or are not possible [(^{i}Pr2PN^{Me}P)Ir]Cl ($\Delta G_{140}^{\ddagger}$ = 30.36 kcal/mol).

INTRODUCTION

There is considerable emphasis on the sustainable and efficient utilization of natural resources that also minimize environmental impact. In this regard, biodiesel stands out as an appealing fuel option, offering environmental advantages in its manufacture, reducing reliance on imported fuel, and being derived from renewable resources.[1] Glycerol plays a pivotal role in the utilization of renewable bio-waste generated as a byproduct in the biodiesel industry.[2] The production of 10 tonnes of biodiesel produces approximately 1 tonne of glycerol (approximately 10% by weight), which can be viewed as an undesirable by-product that is difficult to dispose of without significant environmental impact.[3] An alternative solution for the processing of waste glycerol is either to convert it into valuable products such as propanediol,[4] dihydroxyacetone[5], and lactic acid[6a-c] or to utilize it as a LOHC (liquid organic hydrogen carrier)[6d-f] towards applications in H_2 generation.

Lactic acid is a valuable commodity chemical, with a wide utility in food, pharmaceuticals, chemical industries, cosmetics, biodegradable polythenes, detergents and polylactic acid (PLA) synthesis.[7] The traditional approach to synthesizing lactic acid involves the fermentation of sugars and alcohols.[8] Such processes have relatively low yields and productivity, and require complicated purification and workup. This limits the scalability and cost-effectiveness of producing lactic acid on an industrial scale.[9] Considering these problems, effective methods for producing lactic acid from abundant, waste, glycerol using highly efficient catalysis is of considerable interest.[10]

In 2014, Crabtree and co-workers first reported the use of homogeneous iridium(I) N–heterocyclic carbene pre-catalysts for the acceptorless dehydrogenation of glycerol to form hydrogen and lactic acid. Turnover numbers (TONs) of over 30,000, yields of 91% yield and selectivity of 95% towards lactic acid were reported, Figure 1.[10a] In 2015, Beller and co-workers reported a series of PNP-type pincer ruthenium complexes to catalyze this transformation with 67% yield and 67% selectivity towards lactic acid.[10b] An iron catalyst was developed by Hazari and co-workers using a PNP ligand for glycerol dehydrogenation that gives 24% glycerol conversion with 83% selectivity.[10c] Tu and co-workers carried out the dehydrogenation of glycerol catalyzed by Ir-NHC complex and obtained up to 92% yield and 3266 turnover numbers (TONs) of lactic acid.[10d] In 2016, Williams and co-workers reported a Ir(I) pyridine-NHC complex, where the TONs reached up to 4.5×10^6 in 32 days and a yield of 90% of lactic acid.[10e] In 2018, Voutchkova-Kostal utilized sulfonate-functionalized Ir(I), Ir(III), and Ru(II) NHC complexes for efficient LA synthesis from glycerol.[10f] Very recently, Li studied the conversion of glycerol to lactic acid in water in high yields (ca. 99%) and with excellent selectivity (ca. 99%) that was catalyzed by a water-soluble piano-stool iridium complex.[10g] In 2020, Kumar and co-workers synthesized NNN

pincer-Ru complexes using *bis*(imino)pyridine and 2,6-*bis*(benzimidazole-2-yl)pyridine ligands for transforming glycerol into LA and hydrogen. The best results were achieved with a catalyst [(^{Bim2}NNNRuCl(PPh$_3$)$_2$]Cl, which led to a 90% LA yield with 98% selectivity and 92% conversion of glycerol in an open vessel.[10h] In 2022, Fu and coworkers transformed glycerol into lactic acid using PNP-Mn complexes. They achieved a high yield of 96% with 96% selectivity in 24 hours.[10i] Very recently, Kumar and co-workers reported the use of base metal salts of $CoCl_2$,[10j] $MnCl_2$[10k] and $FeCl_2$[10l] along with the corresponding NNN pincer complexes of the latter two[10k-l] for the efficient transfer dehydrogenation of glycerol to lactic acid.

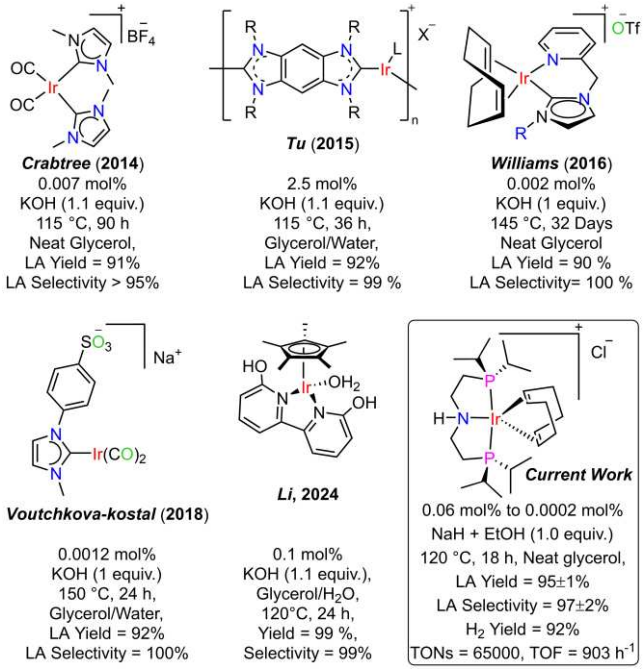

Figure 1. Homogeneous catalytic systems based on Ir reported for the transformation of GLY to LA.[10a,10d-g]

Despite the fact that there has been a recent significant emphasis on catalysis using base-metals,[10m] it is evident from the discussions (*vide-supra*) that catalysts based on Ir[10a,10d-g] have out-performed the rest[10b-c,10h-l] studied towards the acceptorless dehydrogenative transformation of GLY to LA. A brief summary on the homogeneous catalytic systems based on Ir reported for the transformation of GLY to LA is provided in Figure 1. A majority of the Ir based catalysts report prolonged reaction times for the GLY to LA transformation, spanning from 24 hours to 32 days, as well as elevated reaction temperatures, typically in the range of 115-160°C. Additionally, some of these procedures involve the use of co-solvents, such as water, to enhance the solubility of the catalyst and achieve high yields. It would be desirable to formulate the GLY to LA catalytic systems that operate at low temperatures, lower loadings and at shorter reaction times in neat glycerol. Considering the fact there are now straightforward ways to recycle Ir,[10n] the design and development of catalytic systems based on Ir for efficient organic transformations has significant value. In this context, this study now compares the catalytic activity of various PNP pincer-M complexes of the type [(^{iPr2}PN^{H}P)M(L)]X[11a-c] [^{iPr2}PN^{H}P = κ^3-(^{i}Pr$_2$PCH$_2$CH$_2$)$_2$NH; M = Ir, Rh; L = COD and NBD; X$^-$ = Cl$^-$ and [BAr^F]$^-$]. Among the considered catalysts, [(^{iPr2}PN^{H}P)Ir(COD)]Cl at loadings in the range of 0.06-0.0002 mol% is found to promote the GLY to LA transformation, giving a maximum of 95% yield with 97% selectivity towards LA, and turnovers up to 65000 (ToF = 900 h^{-1}) in the presence of an equivalent of *in-situ* generated NaOEt at 120 °C in neat GLY. An inner-sphere mechanism is proposed on the basis of experimental and computational studies, with oxidative addition of glycerol to a 14-electron cationic pincer-Ir intermediate [(^{iPr2}PN^{H}P)Ir]Cl suggested as the RDS. In comparison with the best in the class homogeneous catalytic Ir systems reported previously (Figure 1), the current catalytic system, based on [(^{iPr2}PN^{H}P)Ir(COD)]Cl, demonstrates comparable reactivity, while also offering a comprehensive mechanistic understanding obtained from a combined kinetic and DFT analysis.

RESULTS AND DISCUSSIONS

Studies on the pincer-Ir and pincer-Rh catalyzed acceptorless dehydrogenation of glycerol to lactic acid. We initiated our investigations into the acceptorless dehydrogenation of glycerol to lactic acid with the optimization ^{iPr2}PN^{H}P pincer-iridium and -rhodium catalysts (Figure 2) using one equivalent of either commercially available NaOEt or *in-situ* generated NaOEt (in EtOH) as base. In a typical reaction, 5 mmol of neat glycerol (13.7 M) containing 0.06 mol% (8.2 mM) of the catalysts **1a-c** or **2a** was treated with an equivalent of base and the viscous reaction mixture was heated to 140 °C under an argon atmosphere. The reaction mixture was subsequently cooled after an appropriate time, and an aliquot withdrawn. The yield of sodium salt of lactic acid Na[LA] **4** was determined from ^{1}H NMR using sodium acetate as an external standard.

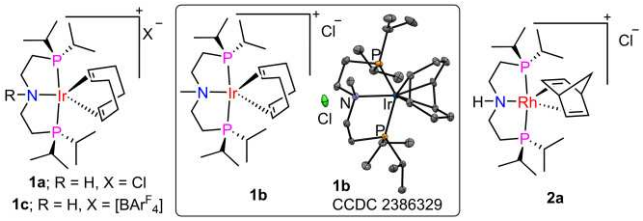

Figure 2. PNP pincer-Ir and pincer-Rh catalysts screened in this current study for the transformation of GLY to LA. The plot of **1b** is provided with displacement ellipsoids drawn at 50% probability.

Among the considered catalysts **1a-c** and **2a**, complex **1a** exhibited the highest catalytic activity and selectivity after 4 h reaction time at 140 °C by employing NaOEt generated *in-situ* from NaH + EtOH (entry 1 Table 1). Utilizing commercially available NaOEt resulted in a lower yield (entry 2 Table1). In order to elucidate the potential impact of the N–H group of the ^{iPr2}PNP ligand on the GLY to Na[LA] conversion, the catalyst with a *N*-methyl-substitution, **1b** was tested. Upon comparing the performance of **1a** and **1b**, it was observed that complex **1b** was not as effective as **1a** in selectivily converting GLY into Na[LA] under identical conditions (entries 3-4 *vs.* entries 1-2, Table 1). This observation suggests a significant influence of the N–H functionality within complex **1a** in this transformation.[11d] The catalytic activity of glycerol dehydrogenation significantly decreased while changing the anion from Cl$^-$ in catalyst **1a** to [BAr^F$_4$]$^-$ in catalyst **1c** (entries 5-6 *vs.* entries 1-2, Table 1). Catalytic reactions carried out with **2a** revealed that an Ir to Rh substitution also leads to poor activity (entries 7-8 *vs.* entries 1-2, Table 1). Under these general reaction conditions, the high selectivity observed for LA suggests that GLY decarbonylation[10] and LA decarboxylation[10], which produces ethylene glycol and FA, respectively, are minimal.

Table 1. The pincer-Ir and pincer-Rh catalyzed dehydrogenation of GLY to LA under varying conditions.[a]

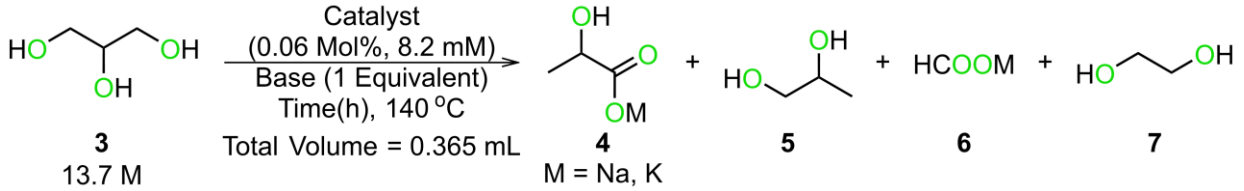

Entry	Catalyst	Base	Temperature (T °C)	Time (h)	Conversion[b] of **3** (%)	% Yield[b] 4	5	6	7	Selectivity[c] towards **4** (%)
1	**1a**	EtOH+NaH	140	4	97	96	Trace	Trace	Trace	99
2	**1a**	NaOEt	140	4	96	84	11	Trace	Trace	86
3	**1b**	EtOH+NaH	140	4	92	70	13	0	0	76
				12	96	87	7	Trace	Trace	88
4	**1b**	NaOEt	140	4	26	13	2	Trace	0	51
				72	97	90	0	Trace	0	93
5	**1c**	EtOH+NaH	140	4	30	11	0	Trace	Trace	35
				96	99	88	0	2	0	89
6	**1c**	NaOEt	140	4	15	3	0	0	0	18
				96	93	75	0	3	0	81
7	**2a**	EtOH+NaH	140	4	0	0	0	0	0	–
				96	93	91	0	0	Trace	98
8	**2a**	NaOEt	140	4	0	0	0	0	0	–
				96	90	88	0	Trace	0	97
9	**1a**	EtOH+NaH	130	12	95	94	0	Trace	Trace	99
10[d]	**1a**	EtOH+NaH	120	18	98±2(92% H_2)	95±1	0	Trace	Trace	97±2
11	**1a**	EtOH+NaH	100	18	79	64	10	Trace	0	82
				30	86	76	5	1	0	92
12	**1a**	NaOEt	120	18	95	90	0	1	Trace	95
13	**1a**	NaO^{t}Bu	120	18	98	94	0	Trace	Trace	96
14	**1a**	KO^{t}Bu	120	18	70	60	6	3	Trace	87
15	**1a**	NaOH	120	18	90	85	0	Trace	Trace	94
16	**1a**	KOH	120	18	47	35	4	Trace	Trace	76
17	**1a**	NaH	120	18	96	84	8	Trace	Trace	87
18	**1a**	No Base	120	18	0	0	0	0	0	–
19	None	EtOH+NaH	120	18	5	3	0	3	0	59
20[e]	**1a**	EtOH+NaH	120	18	95	70	22	Trace	Trace	72
21[f]	**1a**	EtOH+NaH	120	18	84	53	28	Trace	Trace	63
22[g]	**1a**	EtOH+NaH	120	18	25	11	7	Trace	Trace	44
23[h]	**1a**	EtOH+NaH	120	18	97	96	0	Trace	Trace	99
24[i]	**1a**	EtOH+NaH	120	18	13	5	0	4	0	43
				72	18	13	0	Trace	Trace	98
25[j]	**1a**	EtOH+NaH	120	18	49	38	2	Trace	Trace	77
26[k]	**1a**	EtOH+NaH	120	18	89	83	4	0	Trace	93
27[l]	**1a**	EtOH+NaH	120	18	94	86	5	0	Trace	91
28[m]	**1a**	EtOH+NaH	120	18	98	90	9	Trace	Trace	92
29[n]	**1a**	EtOH+NaH	120	18	99	94	4	Trace	Trace	95

[a]Reaction conditions; 5 mmol (13.7 M) of neat glycerol, 0.06 mol% (8.2 mM) of catalyst, 5 mmol of base. Heated to 140 °C. [b]Conversion and yield were determined from ^{1}H NMR using sodium acetate as standard. [c]Selectivity of lactic acid = (yield of LA/conversion of GLY)*100. [d] Result provided as average of four runs. [e]0.75 equivalents of EtOH+NaH were used. [f]0.5 equivalents of EtOH+NaH were used. [g]0.25 equivalents of EtOH+NaH were used. [h]1.25 equivalents of EtOH+NaH were used. [i]0.0002 mol% of **1a** was used. [j]0.002 mol% of **1a** was used. [k]0.02 mol% of **1a** was used. [l]0.04 mol% of **1a** was used. [m]0.08 mol% of **1a** was used. [n]0.1 mol% of **1a** was used.

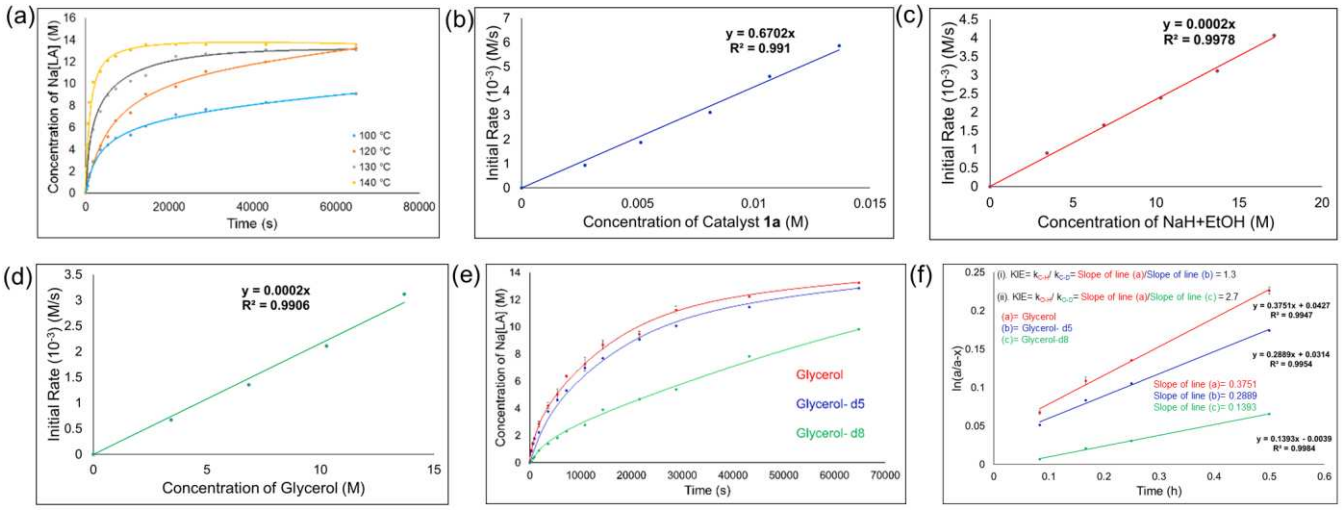

Figure 3. (a) Typical profiles for the formation of Na[LA] vs. time under the reaction conditions for entries 7, 9, 10 and 11 of Table 1. **(b)** Variation of the initial rate of formation of Na[LA] with the concentration of **1a** (reaction conditions: glycerol (0.460 g, 5.0 mmol), *in-situ* generated NaOEt (NaH: EtOH = 0.120 g, 5 mmol: 0.291 mL, 5 mmol) and **1a** (0.02-0.1mol%; 0.00064-0.0032g , 0.001-0.005mmol) at 120 °C). Also see Figure S29. **(c)** Variation of the initial rate of formation of Na[LA] with the concentration of *in-situ* generated NaOEt (reaction conditions: glycerol (0.460g, 5 mmol), catalyst **1a** (0.06 mol%; 0.0019 g, 0.003 mmol), and *in-situ* generated NaOEt (NaH: EtOH = 0.030-0.150 g, 1.25-6.25 mmol: 0.072-0.365 mL, 1.25-6.25 mmol) at 120 °C). Also see Figure S30. **(d)** Variation of the initial rate of formation of Na[LA] with the concentration of glycerol (reaction conditions: glycerol (0.115g- 0.460 g, 1.25-5 mmol), *in-situ* generated NaOEt (NaH: EtOH= 0.120 g, 5 mmol: 0.291 mL, 5 mmol) and 1a (0.06 mol%; 0.0019 g, 0.003 mmol) at 120 °C). Also see Figure S31. (e-f) Determination of kinetic isotope effect for the **1a** catalyzed glycerol dehydrogenation to Na[LA]. (reaction conditions: glycerol/ glycerol-d5/glycerol-d8 (0.460 g, 5.0 mmol), *in-situ* generated NaOEt (NaH: EtOH= 0.120 g, 5 mmol: 0.291 mL, 5 mmol) and **1a** (0.06 mol%; 0.0019 g, 0.003 mmol) at 120 °C). Also see Figure S34.

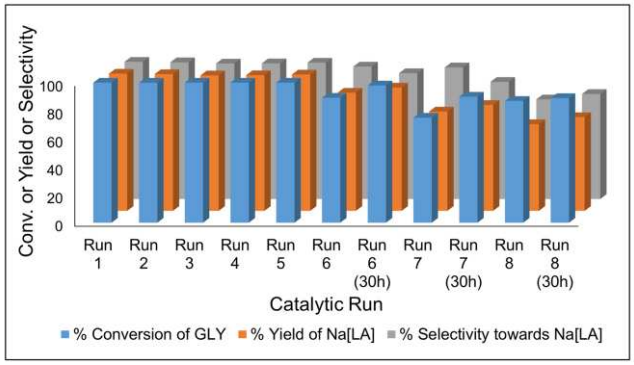

Figure 4. Recharge experiments using catalyst **1a** (reaction conditions: neat glycerol (0.460 g, 5.0 mmol), *in-situ* generated NaOEt (NaH: EtOH= 0.120 g, 5mmol: 0.291mL, 5 mmol) and **1a** (0.06 mol%; 0.0019 g, 0.003 mmol) at 120 °C for the first cycle. Thereafter 5.0 mmol each portion of glycerol and *in-situ* generated NaOEt is added periodically after 18 h for seven more cycles). Also see Table S1.

While catalysis using **1a** is complete within 4h at 140 °C (entry 1, Table 1, Figure 3a and S32), lower reaction temperatures also retain this excellent selectivity: 130 °C (entry 9, Table 1, Figure S32) and 120 °C (entry 10, Table 1, Figure 3a and S32) but take longer to go to completion, 12h and 18h respectively. At 120 °C, four repeat experiments show a very consistent catalytic reaction, with overall conversions between 95-100%, LA yield between 94-95% and selectivity between 95-99% (Table S2). Catalytic dehydrogenation of GLY to Na[LA] was slow at 100 °C (entry 11, Table 1, Figure 3a and S32), and did not reach completion after 30 h. Following these reactions by periodic sampling **1a** (Figure 3a) showed that catalysis at 120 °C (Figure S32) provided a good kinetic profile, and further optimization of the reaction was carried out under these conditions. A 92% yield of hydrogen was also observed under these conditions (Figure S35). The comparable yields of Na[LA] (95%) and H_2 (92%) is indicative of the excellent selectivity and mass-balance obtained in the dehydrogenation of GLY catalyzed by **1a**. Although a detailed determination of catalyst speciation was not possible under these conditions of very low catalyst loadings (0.06 mol%), the possibility of replenishing the system with more substrate post initial reactivity was investigated by repeatedly adding NaH + EtOH and neat glycerol to the reaction mixture after every 18h. Catalyst **1a** could transform replenished GLY across eight consecutive catalytic runs, amounting to a total turnover of 11960 (Figure 4). For the first five runs, **1a** facilitated the complete conversion of glycerol with 99% selectivity toward Na[LA]. After this a gradual decline in measured conversion, and selectivity, was observed (Figure 4). Conversion could however be marginally improved by extending the reaction time to 30 h for the runs 6-8 (Figure 4). These data suggest a slow catalyst deactivation that was not captured in the first runs under the temporal conditions used.[11e]

Scheme 1. Control Experiments

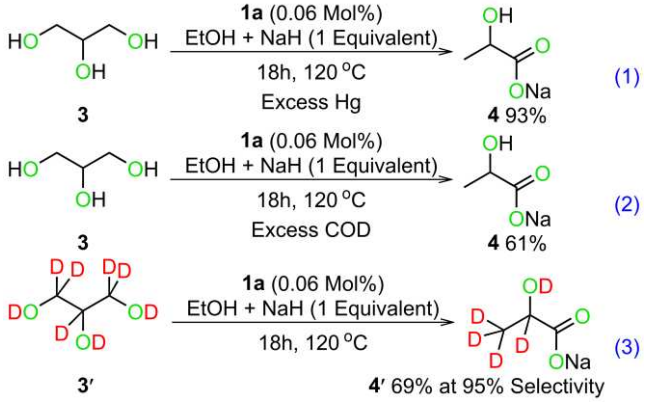

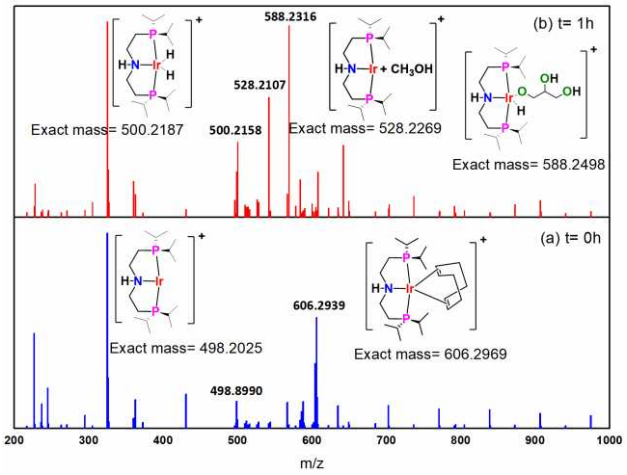

Figure 5. HRMS analysis of the reaction mixture obtained from the **1a** catalyzed transformation of GLY to LA (reaction conditions: glycerol (0.460 g, 5.0 mmol), *in-situ* generated NaOEt (NaH: EtOH= 0.120 g, 5mmol: 0.291mL, 5 mmol) and **1a** (0.06 mol%; 0.0019 g, 0.003 mmol)) after (a) t = 0 h at room temperature and (b) t = 1 h at 120 °C.

The reactivity of commercially available NaO^{t}Bu was comparable to the corresponding activity obtained with in-situ generated NaOEt, albeit with lower selectivity towards Na[LA] (entry 10 vs. entry 13, Table 1), while the commercially available NaOEt and NaOH demonstrated relatively lower Na[LA] yields with moderate selectivity (entry 10 vs. entries 12 and 15, Table 1). KO^{t}Bu and KOH demonstrated poorer activity (entries 14 and 16, Table 1 and Figure S33). To confirm that differences between 'EtOH + NaH' and commercially available NaOEt is not due to a non-negligible amount of NaH remaining in the 'EtOH + NaH' mixture, we performed an additional experiment using commercially available NaH as a base under otherwise standard conditions (entry 17, Table 1). This reaction yielded 84% Na[LA] with 87% selectivity which is lower than the selectivity obtained with in-situ generated NaOEt (entry 10, Table 1). While we currently do not have a definitive explanation for these results, the expedient in-situ generation of NaOEt provides a reliable method to afford high selectivity and conversion (entry 10, Table 1) when compared commercially available NaH (entry 17, Table 1) and NaOEt (entry 12, Table 1). No reactivity was observed in the absence of a base (entry 18, Table 1). Only 3% yield of LA was observed in the absence of **1a** under otherwise identical reaction conditions (entry 19, Table 1).

Control experiments and experimental mechanistic insights. There was a systematic decrease in the initial rate (Figure S30) and yield of LA and associated reduction in selectivity on variation of the amount of *in-situ* generated NaOEt added, from 1.25 equivalents to 0.25 equivalents of (entries 23, 10, 20, 21 and 22, Table 1). These observations highlight the importance of base, not only to generate the catalytically active species (e.g. Scheme 2 and Scheme 3) but also to arrest the LA as the sodium salt, thereby accomplishing an efficient sequestration of glyceraldehyde while mitigating its possible reversible hydrogenation to glycerol. An analysis of the reaction order by the initial-rate method indicated the first-order dependence of initial rate on the concentration of GLY (Figure 3d). While the conversion and selectivity gradually increase when the loading of **1a** was varied from 0.0002 mol% to 0.04 mol% (entries 24-27, Table 1 and Figure S29), any further increase in catalyst loading up to 0.1 mol% did not have a significant effect (entries 10, 28 and 29, Table 1). The initial rates measured for each catalyst concentration varied linearly with the increase in [**1a**] (Figure 3b).

Evidence to the homogeneous molecular nature of the catalytic system was obtained by performing a mercury drop experiment, where a drop of mercury in the **1a** catalyzed transformation of GLY to LA had negligible effect on the measured reactivity (compare entry 10 of Table 1 with equation 1 of Scheme 1). Analysis of the catalysis mixture after 1 hr reaction time using electrospray ionization high resolution mass spectrometry (ESI-HRMS) shows a number of cationic species present of the type [(^{iPr2}PN^{H}P)IrL], at m/z = 500.2158, 528.2107 and 588.2316 for L = $(H)_2$, MeOH and glyceroxide respectively, Figure 5. These replace **1a** [(^{iPr2}PN^{H}P)Ir(COD)]$^+$, which is observed at t = 0 hr. One may note that the three-coordinate pincer-Ir species with m/z = 498.2025 at t = 0h is more likely to be formed owing to the MS acquisition conditions. When catalysis is repeated in the presence of excess COD (equation 2, Scheme 1) diminished conversion is observed after 18 hr, which is indicative of the role of dissociation of COD from **1a** as a key step in the generation of the active catalyst.

The corresponding transformation of per-deuterated glycerol **3'** to deuterated lactate **4'**, in a side-by side experiment,[11f] proceeded at a slower overall rate with a k_H/k_D[11g] value of 2.7 (Figure 3e-f), but also lead to lower yield of 69% albeit with comparable selectivity of 95% (entry 10, Table 1 *vs.* equation 3, Scheme 1). The k_H/k_D of 2.7 is suggestive of either a C–H bond cleavage or an O–H bond cleavage involved in, or prior to, the RDS. In a side-by-side experiment with glycerol **3** and glycerol-D_5 (D_5 = $HOCD_2CD(OH)CD_2OH$) **3''**, a k_H/k_D of 1.3 was measured, which isolates a secondary KIE effect to C–D substitution. The k_H/k_D value of 2.7 obtained in experiments with **3'** thus reflects the additive isotope effect from both the C–H and O–H bonds, with the O-H bond activation as a primary KIE, as is shown from its participation in the RDS as demonstrated in DFT studies (Figure 6 and its discussion, *vide-infra*).

Proposed Mechanism. GLY has two primary hydroxyl (OH) groups and one secondary (-OH) group, which leads to the formation of two possible products: glyceraldehyde (GLA) through the oxidation of one of the primary (-OH) groups, or dihydroxyacetone (DHA) through the oxidation of the secondary (-OH) group. Both transformations have been computed to be thermodynamically endergonic, with GLA being 5.29 kcal/mol above GLY and DHA being 9.83 kcal/mol above GLY. Furthermore, the direct uncatalyzed transformation of GLY to both GLA and DHA are computed to be kinetically unfavorable ($\Delta G_{140}^{\ddagger}$ = 80.20 kcal/mol and 86.26 kcal/mol respectively, Scheme S45). Thus the uncatalyzed transformations of GLY to either GLA or DHA are kinetically and thermodynamically unfavored. While use of catalysts for dehydrogenations have the potential to make these transformations kinetically favorable, open-vessel conditions that remove generated hydrogen and the use of stoichiometric amounts of base to generate the sodium salt of LA, make these reactions thermodynamically favorable.

For the **1a** catalyzed transformation of GLY to LA, several mechanisms can be proposed of which three most plausible mechanisms are shown in Scheme 2-4, and have been examined by using DFT methods.

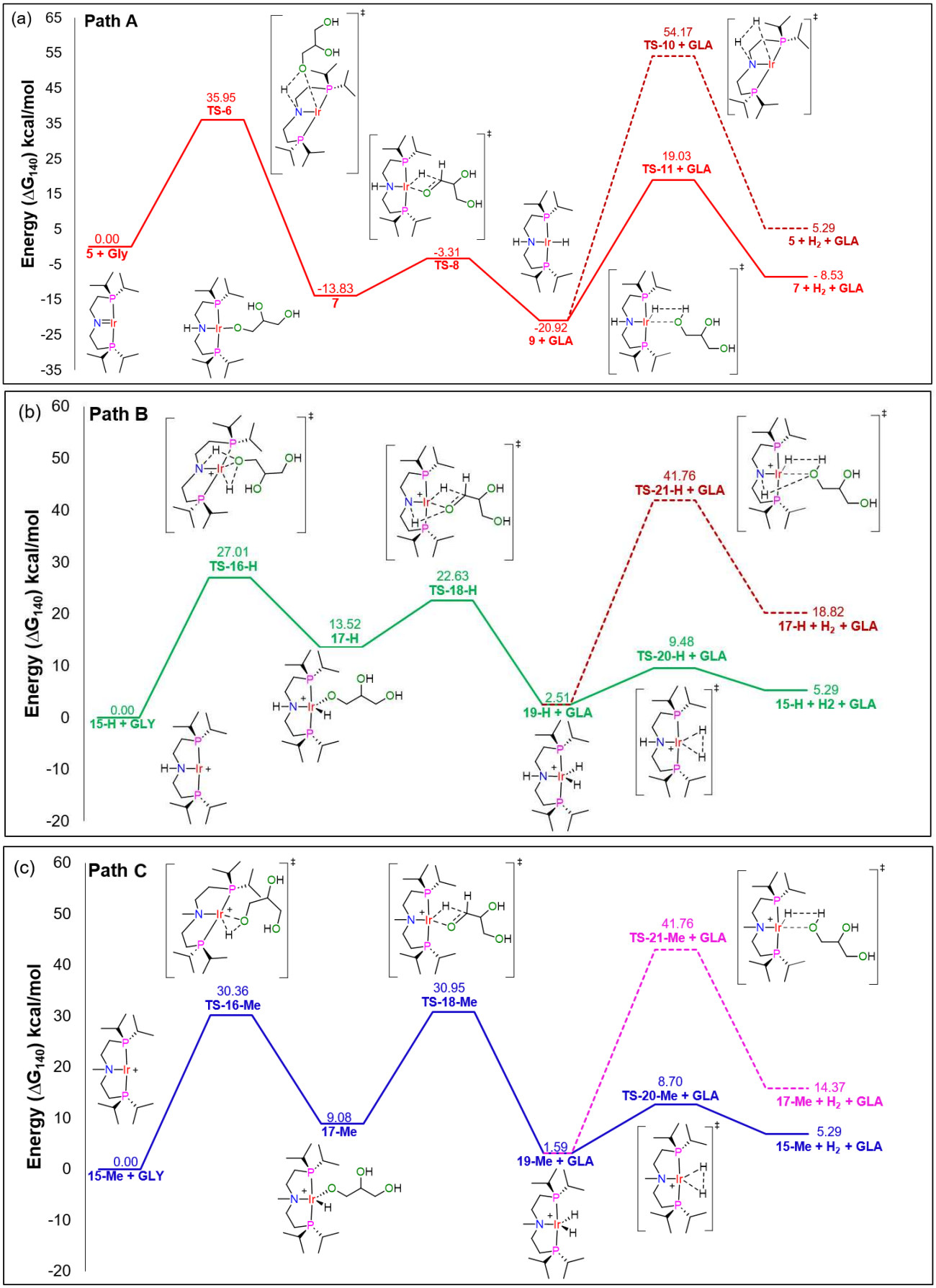

Figure 6. Free energy (ΔG_{140}) profile of various intermediates and TSs in the (a) the **1a** catalyzed GLY to LA reaction via outer-sphere mechanism (**Path A**) (b) the **1a** catalyzed (**Path B**) and (c) the **1b** catalyzed (**Path C**) GLY to LA reaction via an inner-sphere mechanism.

Scheme 2. The 1a Catalyzed GLY to LA Transformation via the Outer-Sphere Mechanism (Path A)

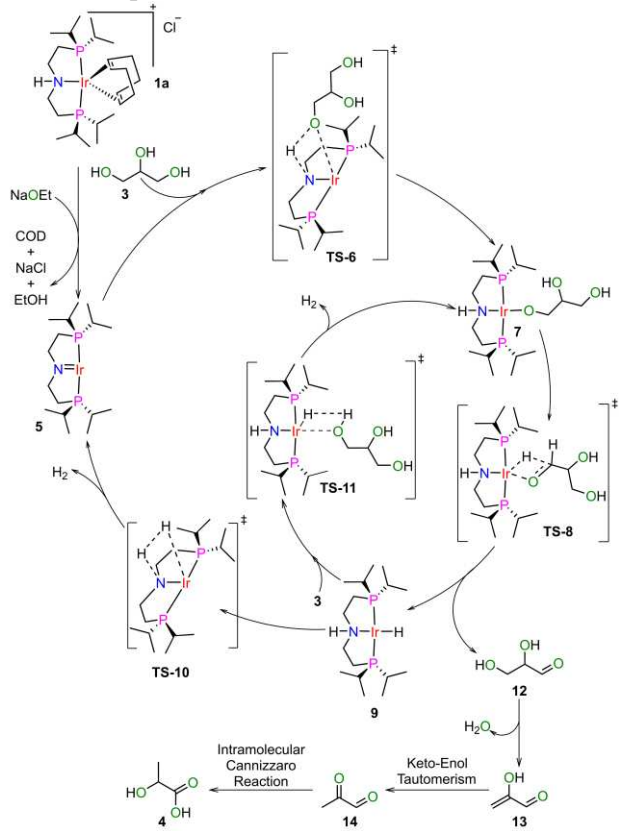

All computations here were performed at 140 °C considering the fact that the **1a** was very efficient under these conditions (entry 1, Table 1, Figure 3a and S32). **Path A** in Scheme 2 and Figure 6a depicts the **1a** catalyzed conversion of GLY to LA via the outer-sphere mechanism.[11b] In this case, a neutral, transient, 14-electron tri-coordinate Ir(I) species **5** can be generated via the dissociation of COD from **1a** and subsequent salt metathesis with NaOEt. Following a MLC path, intermediate **5** can undergo a O–H activation through transition state **TS-6** ($\Delta G_{140}^{\ddagger}$ = 35.95 kcal/mol) to produce the Ir(I) glyceroxide complex **7.** This step is kinetically difficult, but **7** is –13.83 kcal/mol more stable than **5**. Intermediate **7** then undergoes a β-hydride transfer to Ir center through the transition state **TS-8**, having a barrier of 10.52 kcal/mol to form Ir(I) hydride species **9** which is the most stable intermediate, settling at –20.92 kcal/mol below the reference complex **5**. The intermediate **9** has two potential pathways to evolve, the first possibility being a metal-ligand cooperativity (MLC) type H_2 elimination through the transition state TS-10 having a kinetically forbidden barrier ($\Delta G_{140}^{\ddagger}$ = 75.09 kcal/mol) while restoring **5** (Figure 6a).

The second possibility also has a high barrier and involves the alcoholysis of a new GLY through transition state **TS-11** to form **7** with a concomitant liberation of H_2 with a kinetic barrier of 39.95 kcal/mol. **Path A** can thus be ruled out owing to kinetic considerations (Figure 6a). **Path A'** in Figure S36a invokes the formation of DHA via the **Ia** catalyzed reaction and involves energetics of intermediates and TSs that are very similar to **Path A** and is clearly kinetically unfavorable.

Scheme 3 sheds light on an alternative **Path B** where the reactivity is completely based on inner-sphere mechanism. Here one could envisage the catalyst **1a** leading to cationic species **15-H** with a coordinating ethoxide counterion along with the formation of NaCl. One would envisage that the heat of formation of $Na[BAr^F{}_4]$ is relatively unfavorable starting from **1c** which is reflected in its slow reactivity (entries 5 and 6, Table 1). An oxidative addition of the primary hydroxyl of GLY on to the Ir(I) center in **15-H** could lead to Ir(III) glyceroxide species **17-H** with a hydrogen bond interaction between N–H and glyceroxide O (Scheme 3) in an endergonic process (ΔG_{140} = 13.52 kcal/mol). This transition goes through **TS-16-H** and has a barrier of 27.01 kcal/mol (Figure 6b). The barrier is much higher ($\Delta G_{140}^{\ddagger}$ = 31.96 kcal/mol) if a hydrogen-bonded Ir(III) glyceroxide species is not considered (Figure S37). The oxidative addition in the cycle that involves hydrogen bonding (Figure 6b) is more favorable by 4.95 kcal/mol in comparison to the corresponding cycle where hydrogen bonding is not invoked (Figure S37).

Scheme 3. The 1a Catalyzed GLY to LA Transformation via an Inner-Sphere Mechanism (Path B) and by Invoking Hydrogen Bonding

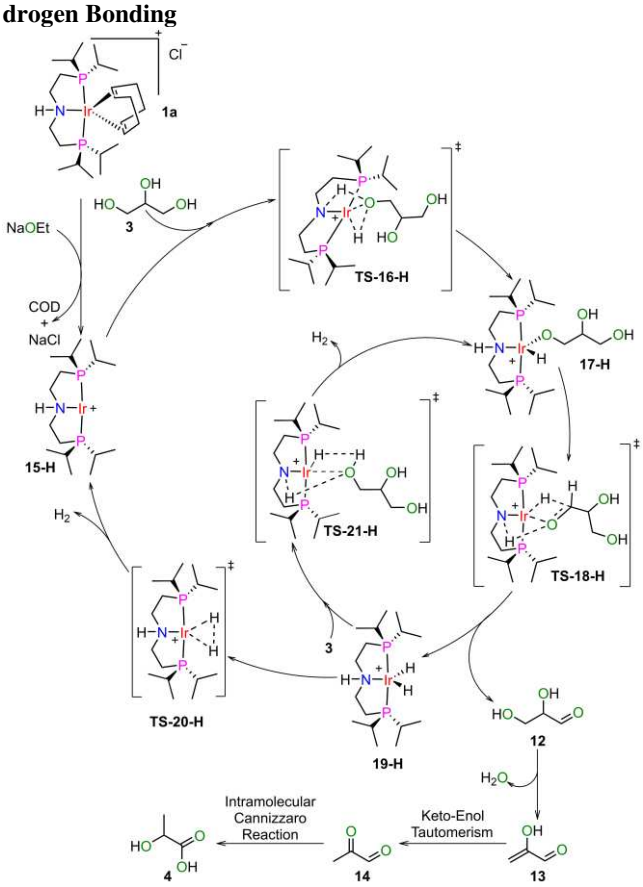

Further, **17-H** may undergo a β-hydride transfer via the transition state **TS-18-H** with a barrier of 9.11 kcal/mol leading to the formation of GLA and a Ir(III) dihydride species **19-H**, which is 2.51 kcal/mol above the reference **15-H** (Figure 6b). The Ir(III) dihydride species **19-H** has two potential pathways. The first possibility is the alcoholysis of **19-H** with a new GLY leading to **17-H** with concomitant release of H_2 via transition state **TS-21-H** with a very high barrier of 39.24 kcal/mol. The high kinetic barrier makes this step less favorable. On the other hand, the reductive elimination of H_2 from **19-H** goes through the transition state **TS-20-H** a with a very reasonable barrier of 6.97 kcal/mol to restore **15-H**.

On a similar note, Scheme 4 discusses the possibility of catalytic cycle via **Path C** using catalyst **1b** (Figure 6c) where inner-

sphere mechanism is the only possibility. Here, the intermediate **15-Me** derived from **1b** with a -NMe group, passes **TS-16-Me** of 30.36 kcal/mol barrier, but ends up in the rather relatively stable Ir(III) glyceroxide intermediate **17-Me**, which is 9.08 kcal/mol above the reference. It is thus apparent that the oxidative addition in the cycle that involves hydrogen bonding (Figure 6b) is more favorable by 3.35 kcal/mol in comparison to the corresponding cycles where there is no possibility (Figure 6c) of hydrogen bonding.

Scheme 4. The 1b Catalyzed GLY to LA Transformation via an Inner-Sphere Mechanism (Path C)

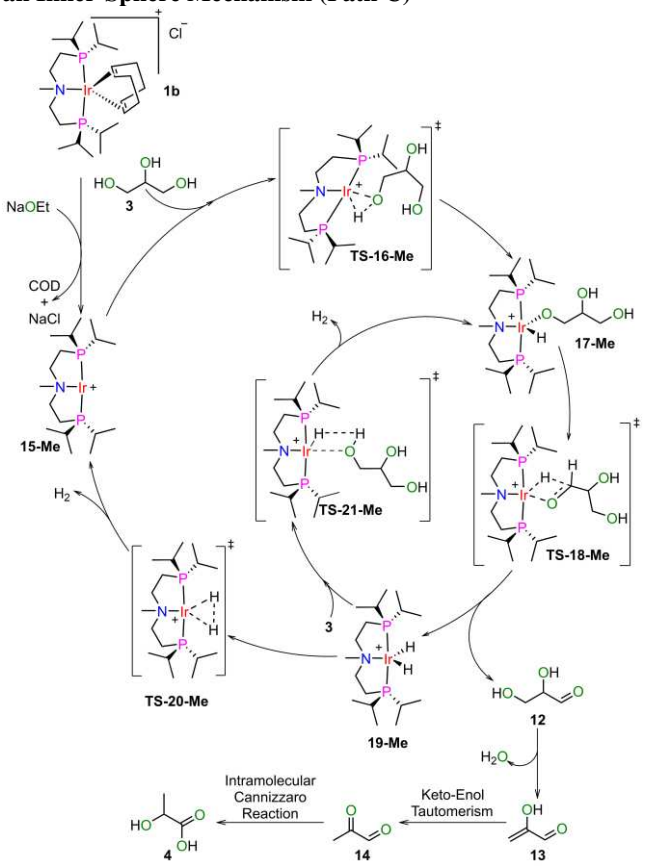

Subsequent β-hydride transfer to form a Ir(III) dihydride species **19-Me** and eliminate GLA through **TS-18-Me** has a much higher barrier of 21.87 kcal/mol (Figure 6c). On one hand, alcoholysis of **19-Me** with a new GLY leading to **17-Me** with concomitant release of H_2 via transition state **TS-21-Me** has a very high barrier of 40.17 kcal/mol which makes these step unfavorable. On the other hand, the reductive elimination of H_2 from **19-Me** goes through the transition state **TS-20-Me** with a more reasonable barrier of 7.11 kcal/mol respectively to restore **15-H** and **15-Me**.

A critical analysis of the various steps involved in the catalytic cycles of **1a** and **1b** provides the necessary explanation on why **1a** is more active than **1b** in transforming GLY to LA while going through the most favorable **Path B** (**15-H→ TS-16-H→ 17-H→TS-18-H→19-H→TS-20-H→15-H**) involving hydrogen bonds between glyceroxide O and NH of the pincer backbone with an overall rate-determining barrier of 27.01 kcal/mol. Interestingly, some of these intermediates are detected by ESI-HRMS analysis (Figure 5). Other possibilities involving DHA via **Path A'** for the catalytic cycle of **1a** (Figure S36a) or via **Path B'** and **Path C'** for the catalytic cycles of **1a** (Figure S36b and Figure S36c) and **1b** (Figure S38) respectively, demonstrate comparable energetics as discussed for the corresponding cycles in **Path A**, **Path B** and **Path C**.

CONCLUSIONS

In conclusion, this study highlights the application of pincer iridium complexes for the catalytic dehydrogenation of glycerol to lactic acid, in particular using pre-catalyst [($^{i\text{Pr}2}$PN$^{\text{H}}$P)Ir(COD)]Cl, **1a** that promotes high conversions (96% yield within 4h) and excellent selectivity (99%) at 140 °C. Mechanistic investigations have provided valuable insights into the reaction mechanism. Evidence for the homogeneous nature of the reaction involving well-defined molecular catalysts was obtained from mercury-drop experiments. The kinetic studies demonstrated a first-order dependence of the rate on the concentration of catalyst **1a**, and glycerol. An inner-sphere mechanism, rather than an outer-sphere mechanism, is suggested to be operative as the former provides an explanation for the performance and activity of [($^{i\text{Pr}2}$PN$^{\text{Me}}$P)Ir(COD)]Cl. Furthermore, DFT studies reveal that the overall energetics via the inner-sphere mechanism are more favorable with oxidative addition of glycerol to a 14-electron pincer-Ir intermediate [($^{i\text{Pr}2}$PN$^{\text{H}}$P)Ir]Cl being identified as the rate-determining step (RDS). Deuterium labeling investigations revealed a k_H/k_D of 2.7 in studies with glycerol-D_8, while a k_H/k_D of 1.3 was obtained with glycerol-D_5. A combined analysis of DFT and isotope-labelling studies reveal that the O–H bond activation participates in the RDS and is the major contributor to the observed KIE of 2.7 with per-deuterated glycerol. The GLY dehydrogenation is kinetically more favorable ($\Delta G_{140}^{\ddagger}$ = 27.01 kcal/mol) when one of the terminal O-H's of glycerol is hydrogen-bonded to the N–H of the pincer backbone. This is in contrast to cases where hydrogen bonds are not possible [($^{i\text{Pr}2}$PN$^{\text{Me}}$P)Ir]Cl ($\Delta G_{140}^{\ddagger}$ = 30.36 kcal/mol) or are not invoked ($\Delta G_{140}^{\ddagger}$ = 31.96 kcal/mol). Overall, this investigation lays the foundation for the development of efficient and sustainable catalytic systems for the conversion of glycerol to lactic acid and hydrogen, contributing to the advancement of green chemistry and the utilization of biomass-derived feedstock in the production of valuable chemicals.

EXPERIMENTAL SECTION

General Procedure and Materials. All manipulations were carried out under purified argon using a standard double manifold or glove box and the catalytic reactions were performed under an argon atmosphere using an oven-dried 5 mL pear-shaped flask attached to a condenser. The chemicals, such as NaO^{t}Bu, KO^{t}Bu, NaOH, KOH, NaH, NaOEt, D_2O, and anhydrous glycerol and glycerol-d8 were purchased either from Sigma-Aldrich or Merck and used as such. The considered catalysts **1a-c** and **2a** along with the ligand PN$^{\text{Me}}$P^{i}Pr were prepared according to the reported protocol.[11a-c] Ethanol was dried and distilled under argon according to the literature procedure.[12]

Physical Measurements. The ^{1}H, ^{2}H, ^{31}P, and ^{13}C{1H} NMR spectra were recorded on a Bruker ASCEND 600 instrument operating at 600 MHz for ^{1}H, 150 MHz for ^{13}C{1H}, and 564 MHz for ^{31}P, or on a Bruker AVANCE 500 instrument operating at 500 MHz for ^{1}H, 125 MHz for ^{13}C{1H} and 470 MHz for ^{31}P, or on a Bruker AVANCE 400 instrument operating at 400 MHz for ^{1}H, 100 MHz for ^{13}C{1H} and 376 MHz for ^{31}P. Chemical shifts (δ) are reported in ppm. Spin-spin coupling constants (J) are expressed in Hz, and other data are reported as follows: s = singlet, d = doubet, t = triplet, m = multiplet, q = quartet, and br = broad singlet.

Synthesis of [Ir(PN$^{\text{Me}}$P^{i}Pr)(COD)]Cl. [Ir(COD)Cl]$_2$ (130 mg, 0.19 mmol) was dissolved in a solution of 1,5 cyclooctadiene (COD, 0.1 cm3, 0.82 mmol) in 3 cm^3 of 1,2-difluorobenzene and then stirred for 1 minute to give a red solution. To this solution, PN$^{\text{Me}}$P^{i}Pr (3.25 cm^3 of

a 0.12 mol dm-3 solution in 1,2-difluorobenzene, 0.39 mmol) was added, upon which the reaction mixture turned yellow. This mixture was then stirred for two hours at room temperature before layering with pentane. Upon diffusion of the pentane, x-ray quality crystals of [Ir(PNMeP^{i}Pr)(COD)]Cl formed. ^{1}H NMR (600 MHz, CD_2Cl_2) 3.43 (br, s, FWHM 150 Hz, 4H, H-10), 2.97 (m, 2H, H-4), 2.90-2.75 (m, 4H, H-2a,2b), 2.39 (br, 4H, H-11a,12a), 2.27 (s, 3H, H-1), 2.12-1.95 (m, 6H, H-3a,3b,H-7), 1.70 (m, br, 4H, H-11b,12b), 1.51 (m, 12H, H-5,6), 1.33 (dd, J = 10.8, 7.2 Hz, 6H, H-8), 1.17 (dd, J = 14.6, 7.5 Hz, 6H, H-9). ^{31}P{^{1}H} NMR (203 MHz, CD_2Cl_2): 22.3. Molecular weight: 655.3045, HRMS (ESI): m/z calculated for [**1b**-Cl]$^+$ = [Ir(PN^{Me}P^{i}Pr)(COD)]$^+$: 620.3126, found 620.3126.

General Procedure for the 1a Catalyzed Glycerol to Lactic Acid Reaction: In a 5mL pear-shaped flask attached to a condenser, neat glycerol (0.460 g, 5 mmol), **1a** (0.06 mol%, 0.0019 g, 0.003 mmol) and *in-situ* generated NaOEt (NaH: EtOH = 0.120 g, 5 mmol: 0.291 mL, 5 mmol) were added inside the glove box and the resulting reaction mixture was heated at 140 °C for 4h. The mixture was then cooled at room temperature and an aliquot was withdrawn from the reaction mixture to an NMR tube containing sodium acetate. The yield of sodium salt of lactic acid was determined by ^{1}H NMR using D_2O as a solvent and sodium acetate as a standard.

General Procedure for the Kinetic Studies

Variation of Catalyst Concentration. To five 5mL pear-shaped flasks attached to a condenser, neat glycerol (0.460g, 5 mmol), and *in-situ* generated NaOEt (NaH: EtOH= 0.120 g, 5 mmol: 0.291 mL, 5 mmol), and various amounts of catalyst (0.02-0.1mol%; 0.00064-0.0032g, 0.001-0.005mmol) were added inside the glove box. The reaction mixture was then heated at 120 °C under an Ar atmosphere. At regular intervals (Figure S29), an aliquot was withdrawn from the reaction mixture and added to an NMR tube containing sodium acetate. The yield of sodium salt of lactic acid was determined by ^{1}H NMR using D_2O as a solvent and sodium acetate as a standard.

Variation of Base Concentration. To four 5mL pear-shaped flasks attached to a condenser, glycerol (0.460g, 5 mmol), catalyst **1a** (0.06 mol%; 0.0019 g; 0.003 mmol), and various amounts of *in-situ* generated NaOEt (NaH: EtOH = 0.030-0.150 g, 1.25-6.25 mmol: 0.072-0.365 mL, 1.25-6.25.00 mmol) were added inside the glove box. The reaction mixture was then heated at 120 °C under an Ar atmosphere. At regular intervals (Figure S30), an aliquot was withdrawn from the reaction mixture and added to an NMR tube containing sodium acetate. The yield of lactic acid was determined by ^{1}H NMR using D_2O as a solvent and sodium acetate as a standard.

Variation of Glycerol Concentration. To four 5mL pear-shaped flasks attached to a condenser, catalyst **1a** (0.06 mol%; 0.0019 g; 0.003 mmol), and *in-situ* generated NaOEt (NaH: EtOH = 0.120 g, 5 mmol: 0.291 mL, 5.00 mmol), and various amounts of glycerol (0.115g-0.460g, 1.25-5 mmol) were added inside the glove box. The reaction mixture was then heated at 120 °C under an Ar atmosphere. *m*-xylene was used as a make-up solvent at a lower concentration of glycerol. At regular intervals (Figure S31), an aliquot was withdrawn from the reaction mixture and added to an NMR tube containing sodium acetate. The yield of sodium salt of lactic acid was determined by ^{1}H NMR using D_2O as a solvent and sodium acetate as a standard.

Computational method: The reaction mechanism and the elementary steps of glycerol oxidation were investigated using density functional theory (DFT) in the Gaussian 09 package,[13] employing the M06[14] functional. For iridium (Ir), the small-core, quasi-relativistic Stuttgart/Dresden effective core potential was utilized with the associated valence basis set (SDD).[15] All other atoms (P, O, C, N, and H) were represented by the 6-311g** basis set[16] in conjunction with empirical dispersion GD3.[17] The singlet, triplet, and quintet spin states were investigated. The transition states were calculated using a synchronous transit-guided quasi-Newton (QST3) approach, and the extrema were verified by analytical frequency calculations. Furthermore, the Intrinsic Reaction Coordinate (IRC) procedure is applied to extrapolate the two minima connected by each transition state. This analysis of the results was based on total energies, including corrections for electronic energies (E) and Gibbs free energies (G) at 413.15 K and 1 atm. The $\Delta G^{\ddagger}$ values were computed assuming an ideal gas, unscaled harmonic vibrational frequencies, and the rigid rotor approximation.

ASSOCIATED CONTENT

Supporting Information

The Supporting Information is available free of charge on the ACS Publications website.

Detailed experimental procedure, NMR of the crude products, GC, HRMS analysis and Cartesian Coordinates. (PDF)

CCDC 2386329 contains the supplementary crystallographic data for this paper. These data can be obtained free of charge via www.ccdc.cam.ac.uk/data_request/cif, or by emailing data_request@ccdc.cam.ac.uk, or by contacting The Cambridge Crystallographic Data Centre, 12 Union Road, Cambridge CB2 1EZ, UK; fax: +44 1223 336033.

AUTHOR INFORMATION

Corresponding Author

* Akshai Kumar − Department of Chemistry, Center for Nanotechnology & Jyoti and Bhupat Mehta School of Health Sciences and Technology, Indian Institute of Technology Guwahati, Guwahati 781039, Assam, India; orcid.org/0000-0002- 3911-3630; Email: akshaikumar@iitg.ac.in

* Andrew S Weller − Department of Chemistry, University of York, York YO10 5DD, UK; orcid.org/ 0000-0003-1646-8081; Email: andrew.weller@york.ac.uk

Author Contributions

V. performed most of the experiments, C.N.B. and M.J.C synthesized all the catalysts. L.K. performed few experiments. F.A.P. assisted in the computational studies and provided key intellectual inputs. A. S. W. and A.K. conceptualized the project and wrote the manuscript.

Funding Sources

Science and Engineering Research Board
Scheme for Transformational and Advanced Research in Sciences, Ministry of Education
Ministry of Electronics and Information Technology
Indian Council of Medical Research
Engineering and Physical Sciences Research Council

Notes

There are no conflicts of interests to declare.

ACKNOWLEDGMENT

V Acknowledges the Department of Science and Technology (DST) for the DST-INSPIRE Research Fellowship (DST/INSPIRE Fellowship/2020/IF200071). A.S.W. is very thankful to EPSRC (ASW) EP/M024210/2 and M.J.C. acknowledges the financial support from the University of York . A.K. is very grateful to the grants received from Science and Engineering Research Board (Grant No. DST-SERB CRG/2022/002354). Thanks are also due to the Scheme for Transformational and Advanced Research in Sciences, Ministry of Education, implemented by Indian Institute of Science (IISc), Bangalore (Grant No. STARS/APR2019/CS/629/FS). A. K. gratefully acknowledges the funds received from Ministry of Electronics and Information Technology via the INUP-I2I program (5(1)/2021-NANO) and the SWASTHA COE (5(1)/2022-NANO). A.K. thanks the financial support from Indian Council of Medical Research, New Delhi (5/3/8/20/2019-ITR). The DST-FIST program, NECBH-IITG, Department of Chemistry at IITG, the Centre for Nanotechnology at IITG and CIF-IITG are acknowledged for various instrumental facilities. PARAM-ISHAN and PARAM-KAMRUP facilities at IITG are gratefully acknowledged for computational facilities.

ABBREVIATIONS

GLY, Glycerol; LA, Lactic Acid; TON, Turnover Number; Turnovers per hour, TOs/h; Rate Determining Step, RDS; Kinetic Isotope Effect, KIE.

REFERENCES

1. Janaun, J.; Ellis, N. Perspectives on biodiesel as a sustainable fuel. *Renew. Sustainable Energy Rev*. **2010**, *14*, 1312–1320.
2. Leoneti, A. B.; Aragã o-Leoneti, V.; Oliveira, S. V. W. B. d.Glycerol as a by-Product of Biodiesel Production in Brazil: Alternatives for the Use of Unrefined Glycerol. *Renewable Energy* **2012**, *45*, 138−145.
3. Dasari, M. A.; Kiatsimkul, P.-P.; Sutterlin, W. R.; Suppes, G. J.Low-Pressure Hydrogenolysis of Glycerol to Propylene Glycol. *Appl.Catal., A* **2005**, *281* (1−2), 225−231
4. (a) Lao, D. B.; Owens, A. C. E.; Heinekey, D. M.; Goldberg, K. I. Partial Deoxygenation of Glycerol Catalyzed by Iridium Pincer Complexes. *ACS Catal.* **2013**, *3*, 2391-2396. (b) Falcone, D. D.; Hack, J. H.; Klyushin, A. Y.; Knop-Gericke, A.; Schlögl, R.; Davis, R. J. Evidence for the Bifunctional Nature of Pt–Re Catalysts for Selective Glycerol Hydrogenolysis. *ACS Catal.* **2015**, *5*, 5679-5695. (c) Zhao, X.; Wang, J.; Yang, M.; Lei, N.; Li, L.; Hou, B.; Miao, S.; Pan, X.; Wang, A.; Zhang, T. Selective Hydrogenolysis of Glycerol to 1,3-Propanediol: Manipulating the Frustrated Lewis Pairs by Introducing Gold to Pt/WOx. *ChemSusChem*. **2017**, *10*, 819-824. (d) Sun, Q.; Wang, S.; Liu, H. Selective Hydrogenolysis of Glycerol to Propylene Glycol on Supported Pd Catalysts: Promoting Effects of ZnO and Mechanistic Assessment of Active PdZn Alloy Surfaces. *ACS Catal.* **2017**, *7*, 4265-4275. (e) Sherbi, M.; Wesner, A.; Wisniewski, V. K.; Bukowski, A.; Velichkova, H.; Fiedler, B.; Albert, J. Superior CNT-supported bimetallic RuCu catalyst for the highly selective hydrogenolysis of glycerol to 1,2-propanediol. *Catal. Sci. Technol.* **2021**, *11*, 6649-6653.
5. (a) Painter, R. M.; Pearson, D. M.; Waymouth, R. M. Selective Catalytic Oxidation of Glycerol to Dihydroxyacetone. *Angew. Chem. Int. Ed.* **2010**, *49*, 9456-9459. (b) Crotti, C.; Kašpar, J.; Farnetti, E. Dehydrogenation of glycerol to dihydroxyacetone catalyzed by iridium complexes with P–N ligands. *Green Chem.* **2010**, *12*, 1295-1300. (c) Chung, K.; Banik, S. M.; De Crisci, A. G.; Pearson, D. M.; Blake, T. R.; Olsson, J. V.; Ingram, A. J.; Zare, R. N.; Waymouth, R. M. Chemoselective Pd-Catalyzed Oxidation of Polyols: Synthetic Scope and Mechanistic Studies. *J. Am. Chem. Soc.* **2013**, *135*, 7593-7602. (d) Liu, S.-S.; Sun, K.-Q.; Xu, B.-Q. Specific Selectivity of Au-Catalyzed Oxidation of Glycerol and Other C3-Polyols in Water without the Presence of a Base. *ACS Catal.* **2014**, *4*, 2226-2230. (e) Gupta, N.; Khavryuchenko, O.; Villa, A.; Su, D. Metal-Free Oxidation of Glycerol over Nitrogen-Containing Carbon Nanotubes. *ChemSusChem* **2017**, *10*, 3030-3034.
6. (a) Lam, C. H.; Bloomfield, A. J.; Anastas, P. T. A switchable route to valuable commodity chemicals from glycerol via electrocatalytic oxidation with an earth abundant metal oxidation catalyst. *ChemSusChem* **2017**, *19*, 1958-1968. (b) Jiang, Z.; Zhang, Z.; Wu, T.; Zhang, P.; Song, J.; Xie, C.; Han, B. Efficient Generation of Lactic Acid from Glycerol over a Ru-Zn-CuI/Hydroxyapatite Catalyst. *Chem. Asian J.* **2017**, *12*, 1598-1604. (c) Ainembabazi, D.; Wang, K.; Finn, M.; Ridenour, J.; Voutchkova-Kostal, A. Efficient transfer hydrogenation of carbonate salts from glycerol using water-soluble iridium N-heterocyclic carbene catalysts. *Green Chem.* **2020**, *22*, 6093-6104. (d) Kumar, A.; Daw, P.; Milstein, D. Homogeneous Catalysis for Sustainable Energy: Hydrogen and Methanol Economies, Fuels from Biomass, and Related Topics. *Chem. Rev.* **2022**, *122*, 385−441. (e) Yadav, V.; Sivakumar, G.; Gupta, V.; Balaraman, E. Recent Advances in Liquid Organic Hydrogen Carriers: An Alcohol-Based Hydrogen Economy. *ACS Catal.* **2021**, *11*, 14712−14726. (f) Bisarya, A.; Karim, S.; Narjinari, H.; Banerjee, A.; Arora, V.; Dhole, S.; Dutta, A.; Kumar, A. Production of hydrogen from alcohols via homogeneous catalytic transformations mediated by molecular transition-metal complexes. *Chem. Commun.*, **2024**, *60*, 4148–4169.
7. (a) Dusselier, M.; Van Wouwe, P.; Dewaele, A.; Makshina, E.; Sels, B. F. Lactic acid as a platform chemical in the biobased economy: the role of chemocatalysis. *Energy Environ. Sci.* **2013**, *6*, 1415-1442. (b) Komesu, A.; de Oliveira, J. A. R.; da Silva Martins, L. H.; Maciel, M. R. W.; Maciel Filho, R. Lactic Acid Production to Purification: *A Review. Bioresour.* **2017**, *12*, 4364-4383.
8. He, W.; Li, G.; Kong, L.; Wang, H.; Huang, J.; Xu, J.Application of hydrothermal reaction in resource recovery of organic wastes. *Resour. Conserv. Recycl.* **2008**, *52* (5), 691−699
9. Abdel-Rahman, M. A.; Sonomoto, K. Opportunities to overcome the current limitations and challenges for efficient microbial production of optically pure lactic acid. *J. Biotechnol.* **2016**, *236*, 176−192.
10. (a) Sharninghausen, L. S.; Campos, J.; Manas, M. G.; Crabtree, R. H. Efficient selective and atom economic catalytic conversion of glycerol to lactic acid. *Nat. Commun.* **2014**, *5*, 5084. (b) Li, Y.; Nielsen, M.; Li, B.; Dixneuf, P. H.; Junge, H.; Beller, M. Ruthenium-catalyzed hydrogen generation from glycerol and selective synthesis of lactic acid. *Green Chem.* **2015**, *17*, 193-198. (c) Sharninghausen, L. S.; Mercado, B. Q.; Crabtree, R. H.; Hazari, N. Selective conversion of glycerol to lactic acid with iron pincer precatalysts. *Chem. Commun.* **2015**, *51*, 16201-16204. (d) Sun, Z.; Liu, Y.; Chen, J.; Huang, C.; Tu, T. Robust Iridium Coordination Polymers: Highly Selective, Efficient, and Recyclable Catalysts for Oxidative Conversion of Glycerol to Potassium Lactate with Dihydrogen Liberation. *ACS Catal.* **2015**, *5*, 6573-6578. (e) Lu, Z.; Demianets, I.; Hamze, R.; Terrile, N. J.; Williams, T. J. A Prolific Catalyst for Selective Conversion of Neat Glycerol to Lactic Acid. *ACS Catal.* **2016**, *6*, 2014-2017. (f) Finn, M.; Ridenour, J. A.; Heltzel, J.; Cahill, C.; Voutchkova-Kostal, A. Next-Generation Water-Soluble Homogeneous Catalysts for Conversion of Glycerol to Lactic Acid. *Organometallics* **2018**, *37*, 1400-1409. (g) Xu, X.; You, H.; Dong, B.; He, Y.; Li, F. Selective Conversion of Glycerol to Lactic Acid in Water via Acceptorless Dehydrogenation Catalyzed by a Water-Soluble Metal−Ligand Bifunctional Iridium Catalyst. *Inorg. Chem.* **2024**, *63*, 12929−12934. (h) Dutta, M.; Das, K.; Prathapa, S. J.; Srivastava, H. K.; Kumar, A. Selective and high yield transformation of glycerol to lactic acid using NNN pincer ruthenium catalysts. *Chem. Commun.* **2020**, *56*, 9886-9889. (i) Deng, C.-Q.; Deng, J.; Fu, Y. Manganese-catalysed dehydrogenative oxidation of glycerol to lactic acid. *Green Chem.* **2022**, *24*, 8477-8483. (j) Narjinari, H.; Dhole, S.; Kumar, A. Acceptorless or Transfer Dehydrogenation of Glycerol Catalyzed by Base Metal Salt Cobaltous Chloride–Facile Access to Lactic Acid and Hydrogen or Isopropanol. *Chem. Eur J.* **2024** *30*(1), e202302686. (k) Bisarya, A.; Dhole, S.; Kumar, A. Efficient net transfer-dehydrogenation of glycerol: NNN pincer–Mn and manganese chloride as a catalyst unlocks the effortless production of lactic acid and isopropanol. *Dalton Trans.* **2024**, 10.1039/d4dt01731e. (l) Venkateshappa, B.; Bisarya, A.; Nandi, P. G.; Dhole, S.; Kumar, A.; Production of Lactic Acid via Catalytic Transfer Dehydrogenation of Glycerol Catalyzed by Base Metal Salt Ferrous Chloride and Its NNN Pincer-Iron Complexes. *Inorg. Chem.* **2024**, *63*, 15294-15310. (m) John-Campbell, S. S.; Bull, J. A. Base Metal Catalysis in Directed C(sp3)−H Functionalisation. *Adv. Synth. Catal.* **2019**, *361*, 3662−3682. (n) Cherepakhin, V.; Williams, T. J. Recycling organoiridium waste to [(1,5-cyclooctadiene)IrCl]$_2$. *Green Chem*., **2024**, *26*, 3146-3148.
11. (a) Brodie, C. N.; Sotorrios, L.; Boyd, T. M.; Macgregor, S. A.; Weller, A. S., Dehydropolymerization of H3B·NMeH2 Mediated by Cationic Iridium(III) Precatalysts Bearing κ3-iPr-PNRP Pincer Ligands (R = H, Me): An Unexpected Inner-Sphere Mechanism. *ACS Catal.*, **2022**, *12*, 13050-13064 (b) Brodie, C. N.; Boyd, T. M.; Sotorríos, L.; Ryan, D. E.; Magee, E.; Huband, S.; Town, J. S.; Lloyd-Jones, G. C.; Haddleton, D. M.; Macgregor, S. A.; Weller, A. S. Controlled Synthesis of Well-Defined Polyaminoboranes on Scale Using a Robust and Efficient Catalyst. *J. Am. Chem. Soc.* **2021**, *143*, 21010– 21023 (c) Werkmeister, S.; Junge, K.; Wendt, B.; Alberico, E.; Jiao, H.; Baumann, W.; Junge, H.; Gallou, F.; Beller, M. Hydrogenation of Esters to Alcohols with a Well-Defined Iron Complex.. *Angew. Chemie - Int. Ed*. **2014**, *53*, 8722–8726. (d)

Dub, P. A.; Scott, B. L.; Gordon, J. C. Why Does Alkylation of the N-H Functionality within M/NH Bifunctional Noyori-TypeCatalysts Lead to Turnover? *J. Am. Chem. Soc.* **2017**, *139* (3), 1245−1260. (e) Scott, S. L. A Matter of Life(Time) and Death. *ACS Catal.* **2018**, *8* (9), 8597– 8599. (f) Simmons, E. M.; Hartwig, J. F. On the Interpretation of Deuterium Kinetic Isotope Effects in C-H Bond Functionalizations by Transition-Metal Complexes. Angew. Chem., Int. Ed. 2012, 51, 3066– 3072. (g) Ganguli, K.; Mandal, A.; Kundu, S. Well-Defined Bis(NHC)Mn(I) Complex Catalyzed Tandem Transformation of α,β-Unsaturated Ketones to α-Methylated Ketones Using Methanol. *ACS Catal.* **2022**, *12*, 12444– 12457. (h) Dub, P. A.; Gordon, J. C. Metal–Ligand Bifunctional Catalysis: The "Accepted" Mechanism, the Issue of Concertedness, and the Function of the Ligand in Catalytic Cycles Involving Hydrogen Atoms. *ACS Catal.* **2017**, *7*, 6635–6655.

12. Purification of Laboratory Chemicals; Armarego, W. L. F., Perrin, D. D., Eds.; Butterworth-Heinemann: Woburn, MA, **2000**.
13. Frisch, M. J.; Trucks, G. W., Schlegel, H. B.; Scuseria, G. E.; Robb, M. A.; Cheeseman, J. R.; Scalmani, G.; Barone, V.; Mennucci, B.; Petersson, G. A.; Nakatsuji, H.; Caricato, M.; Li, X.; Hratchian, H. P.; Izmaylov, A. F.; Bloino, J.; Zheng, G.; Sonnenberg, J. L.; Hada, M.; Ehara, M.; Toyota, K.; Fukuda, R.; Hasegawa, J.; Ishida, M.; Nakajima, T.; Honda, Y.; Kitao, O.; Nakai, H.; Vreven, T.; Montgomery, J. A., Jr.; Peralta, J. E.; Ogliaro, F.; Bearpark, M.; Heyd, J. J.; Brothers, E.; Kudin, K. N.; Staroverov, V. N.; Keith, T.; Kobayashi, R.; Normand, J.; Raghavachari, K.; Re dell, A.; Burant, J. C.; Iyengar, S. S.; Tomasi, J.; Cossi, M.; Rega, N.; Millam, J. M.; Klene, M.; Knox, J. E.; Cross, J. B.; Bakken, V.; Adamo, C.; Jaramillo, J.; Gomperts, R.; Stratmann, R. E.; Yazyev, O.; Austin, A. J.; Cammi, R.; Pomelli, C.; Ochterski, J. W.; Martin, R. L.; Morokuma, K.; Zakrzewski, V. G.; Voth, G. A.; Salvador, P.; Dannenberg, J. J.; Dapprich, S.; Daniels, A. D.; Farkas, O.; Foresman, J. B.; Ortiz, J. V.; Cioslowski, J.; Fox, D. J. *Gaussian 09*, Revision D.01; Gaussian, Inc.: Wallingford, CT, 2013.
14. (a) Zhao, Y.; Truhlar, D.G. A new local density functional for main-group thermochemistry, transition metal bonding, thermochemical kinetics, and noncovalent interactions. *J. Chem. Phys.* **2006**, *125*, 194101. (b) Zhao, Y., Truhlar, D.G. The M06 suite of density functionals for main group thermochemistry, thermochemical kinetics, noncovalent interactions, excited states, and transition elements: two new functionals and systematic testing of four M06-class functionals and 12 other functionals. *Theor Chem Account* **2008**, *120*, 215–241.
15. (a) Hay, P.J.; Wadt, W.R. Ab initio effective core potentials for molecular calculations. Potentials for the transition metal atoms Sc to Hg. *J. Chem. Phys.* **1985**, *82*, 270–283. (b) D. Andrae, U. Haussermann, M. Dolg, H. Stoll, H. Preuss, *Theor Chim Acta* **1990**, *77*, 123-141; (c) A. W. Ehlers, G. Frenking, *J Chem Soc Chem Comm* **1993**, 1709-1711; (d) A. Hollwarth, M. Bohme, S. Dapprich, A. W. Ehlers, A. Gobbi, V. Jonas, K. F. Kohler, R. Stegmann, A. Veldkamp, G. Frenking, *Chem Phys Lett* **1993**, *208*, 237-240.
16. (a) Krishnan, R. ; Binkley, J. S.; Seeger, R.; Pople, J. A. Self-consistent molecular orbital methods. XX. A basis set for correlated wave functions*J. Chem. Phys.*, **1980**, *72*, 650-54. (b) McLean, A. D.; Chandler, G. S; Contracted Gaussian basis sets for molecular calculations. I. Second row atoms, *Z*=11–18. *J. Chem. Phys.*, **72** (1980) 5639-48.
17. Grimme, S.; Antony, J.; Ehrlich, S.; Krieg, H. A consistent and accurate ab initio parametrization of density functional dispersion correction (DFT-D) for the 94 elements H-Pu. *J. Chem. Phys.* **2010**, *132*, 154104.

For Table of Contents Entry Only